Monte Carlo Simulation of Small Silicon Mosfet's

Enrico Sangiorgi

Department of Electronics, University of Bologna, Italy

Abstract

In this paper the two dimensional Monte Carlo device simulator BEBOP, developed for silicon devices, is described. The simulator solves self-consistently Boltzmann and Poisson equations for electron and holes starting from a drift-diffusionn initial guess. Bebop can use different isotropic energy vs. wave vector dispersion relationships that try to reproduce the detailed features of the anisotropic silicon band structure. The program is applied to the study of nonequilibrium effects in short channel Mosfet's.

1 Introduction

The progressive scaling down of modern semiconductor devices and circuits enhances the need of more accurate simulation tools able to describe a range of so called *mesoscopic* phenomena which arise when the size of the system is in the order of the characteristic length associated with certain scattering processes. A well known example is, for instance, the velocity overshoot. An ideal method to describe such phenomena in the approximation of the quasi-classical carrier transport is the use of Monte Carlo method to solve the Boltzmann transport equation by simulating a large number of carriers subject to external forces (electric fields) and given scattering mechanisms.

In this framework the Monte Carlo device simulator BEBOP, developed for silicon devices, solves self-consistently Boltzmann and Poisson equations for electron and holes in a two dimensional space domain, starting from an initial guess for electric field and carrier concentration given by a drift-diffusion simulator.

BEBOP can use different isotropic energy vs. wave vector dispersion relationships ($E(k)$) [1, 2, 3], that try to reproduce with different levels of accuracy the detailed features of the anisotropic silicon band structure. The band structure is implemented via a set of cubic spline functions, hence analytical as well as non-analytical $E(k)$ relationships can be accurately and efficiently implemented.

The included scattering mechanisms are electron-phonon, impact-ionization, ionized impurities, and surface scattering; the implementation of electron-electron and electron-plasmon interactions are currently in progress.

The program exploits *ad hoc* techniques for the enhancement of rare events [4, 5]. Such techniques are used to deal with scarcely populated regions in order to keep constant the statistical error in the region of current flow in spite of large spacial variations of doping and carrier concentrations, and in order to enhance statistics related to very energetic carriers. Self consistency between Boltzmann and Poisson equations is achieved by means of an original and efficient coupling scheme presented in [5].

In the following section, the most recent improvements to the simulator in terms of physical models will be presented. Section three reports some results of applications to the study of strong non-equilibrium effects affecting charge transport in deep submicron MOSFETS.

2 Physical models

The band model traditionally used to simulate electron transport in Si includes only the lowest set of minima of the conduction band extended to higher energies through the nonparabolic approximation [6]. This approach is not adequate to describe the physical properties of electrons with energies in excess of $\approx 1eV$. A solution to this problem implies the use of the complete anisotropic semiconductor band structure ($ASBS$) [7, 8], but this is very CPU time consuming because of the anisotropic dispersion relationship $E(\vec{k})$. A good alternative is provided by multiband isotropic models [1, 2, 3, 9] which accurately describe transport phenomena in semiconductors, are significantly less CPU-time consuming, and can be easily implemented in alternative methods to solve Boltzmann transport equation [10, 11].

In particular the models of Refs.[1, 2] are given in terms of analytical electron and hole bands that fit the $ASBS$ density of states (DOS) as a function of energy. The DOS contains *integrated* informations over the $ASBS$ and, in particular, the electron-phonon scattering rate at a given energy is proportional to the DOS of the final state. Therefore, the fitting of the DOS ensures that the simplified models feature the same *average* electron-phonon scattering rate of the more complex $ASBS$. The model of Ref.[1] features an electron band structure consisting of three isotropic parabolic upper bands (two of them are "hole like") together with the usual lowest non-parabolic one in a finite spherical Brillouin zone. The bands are given by analytical expressions whose parameters have been determined by best fitting the $DOS(E)$ up to $3eV$.

Fig.1 shows the DOS obtained from: this model, the $ASBS$, and a single, nonparabolic band model [6]. While the one-band model is inadequate above $1.5eV$ because of its DOS monotonicity, the good agreement between the two former curves indicates that the main effects of the Si band structure are well taken into account. Due to symmetry in the Brillouin zone (BZ), each band is made up of several valleys along the equivalent directions, and a multiplicity factor is used to consider all the available electron states.

Following the same guidelines a multiband model for holes has been developed. It includes four isotropic bands in a finite spherical BZ. Again the four bands provide a best fit to the DOS(E) obtained from an $ASBS$. The analytical dependence $E(\vec{k})$ was obtained by using the non parabolic approximation [6] where the non parabolicity parameter, the effective mass and the geometrical multiplicity factor are not constant along the two bands, in order to account for the warping of the real band structure. Fig.2 shows the considered band structures for electron and holes.

The fitting of the DOS, however, does not ensure that carrier velocity is properly treated. Notice that the carrier velocity in the $ASBS$ ($u_g(\vec{k}) = \frac{1}{\hbar}\nabla_{\vec{k}}E(\vec{k})$) is a function of the wave vector $\vec{k}$, while for any isotropic band model it depends on the magnitude of $\vec{k}$ only, thus on the energy E. Therefore a comparison between the carrier velocity of $ASBS$ and that of isotropic models can be done only through a suitable average group velocity $u_g(E)$. In this framework, we have developed a more complex isotropic band model for electrons and holes in silicon, conceived to best fit the behavior in energy of both DOS and u_g calculated from the $ASBS$. In this case the $E(k)$ relationship is given in terms of numerical isotropic bands, one for each of the main symmetry points in the conduction and the valence band.

From the $E(\vec{k})$ data computed using empirical pseudo-potentials [12], $DOS(E)$ and $u_g(E)$ were obtained following [13]; $u_g(E)$ has been defined weighting all the $u_g(\vec{k})$ by the DOS of the infinitesimal volume around $\vec{k}$, where the $\vec{k}$ are all the momentum vectors lying on the surface at energy E. Fig.3 shows the comparison between the electron $u_g(E)$, computed from the $ASBS$ as shown above, with that provided by uniform MC simulations using directly the $ASBS$ [8]. The excellent agreement between these two quantities demonstrate that, at least for the homogeneous silicon case, the *average* magnitude of $u_g(E)$ is marginally affected by anisotropic field-driven effects.

The isotropic band model has been obtained using the following procedure. The irreducible wedge of the first Brillouin zone was divided into three parts ($\mathcal{P}_i, i = 1,3$), each of them centered on a selected $\vec{k}_{ci}$ and made up of all the nearest $\vec{k}$ vectors. The $\vec{k}_{ci}$ vectors were chosen at the local energy minima (maxima) of the conduction (valence) band: 0.85X, Γ, and L for electrons; X, Γ, and L for holes. This

allows to determine a single isotropic band for each symmetry point, with the same effective mass at $\vec{k}_{ci}$ and multiplicity of the corresponding symmetry point in the $ASBS$. For each region $\mathcal{P}_i$ in the $\vec{k}$ space, the corresponding $DOS_i(E)$ and $u_{gi}(E)$ were calculated integrating over all the $\vec{k}$ states in the $\mathcal{P}_i$ region. Next we computed a set of $E_i(k)$ featuring isotropic DOS_i^{iso} and u_{gi}^{iso} in good agreement with the corresponding DOS_i and u_{gi}, respectively. Since the functions $E_i(k)$ are isotropic, DOS_i^{iso} and u_{gi}^{iso} can be easily obtained analytically [3]. This allows to write a set of two differential equations in the unknown function $E_i(k)$, that cannot be solved exactly. An optimum solution can be found which minimizes the weighted sum of the relative errors made on the DOS and u_g, respectively.

The resulting isotropic band structure for electron and holes is reported in Fig.4. The numerical implementation of the multiband model in the MC device simulator exploits a set of cubic spline functions to represent the $E(k)$ relationship. Since this approach avoids the use of computational intensive mathematical functions and does not require different calculations for analytical and numerical bands, the CPU requirements do not increase compared to the case of a single band [5]. The multiband models are consistently used in the evaluation of the electron-phonon scattering probabilities and the following mechanisms are considered : intraband acoustic scattering in the elastic approximation, optical-phonon scattering to equivalent bands, and interband optical-phonon scattering. The formulae to compute the electron-phonon scattering rates $P(\vec{k},\vec{k}')$ has been extended from the well known analytic band cases to the case where $E(k)$ is given by means of numerical tables, as in our models. This extension was made integrating the $P(\vec{k},\vec{k}')$ expressions [6] over the $\vec{k}$ state space generated by our $E(k)$ functions. The other scattering mechanisms included in the calculations are: a) impact ionization implemented using non-isotropic model of Ref.[14] for the electron multiband model of Ref.[1] or the Keldysh formulation for the other multiband models; b) ionized impurity scattering (Brooks-Herring model); c) surface scattering as a combination of specular and diffusive scattering [15]. For each model phonon coupling constants and temperatures have been determined, when possible, by best fitting available experimental data on transport properties.

3 Results

A set of optimized transport parameters has been obtained for the electron band model of [1] by comparing simulation results with an extended set of experimental data including n-MOSFET substrate current and electron injection probabilities from Si into SiO_2 [16]. The set of transport parameters includes: acoustic phonon ($\mathcal{E}_1$) and optical phonon (D_tK) coupling constants for both intra- and inter-band transitions and the pre-factor (P_{II}) for II probability. As an example, the accuracy of the model in the calculation of the electron energy tail is checked by a comparison of simulations with the experimental data reported in [17], where injection probabilities of photo-generated electrons accelerated in the depletion layer of MOS transistors have been measured. Fig.5 reports a comparison between the measured and calculated injection probabilities: the agreement is excellent over four orders of magnitude. The MC simulator with the electron multiband model of Ref.[1] has been used to study the inpact of voltage scaling on device performance in submicrometer MOSFET's [18]. To this purpose, a reference $1\mu m$ process ($L_{eff} = 0.75\mu m$) has been scaled to $L_{eff} = 0.25\mu m$; using the same process, devices with L_{eff} down to $0.075\mu m$ have been simulated. We investigated two scaling strategies for the applied voltages: the traditional approach (hereafter called F_{av} scaling) aimed to maintain the same value of the average lateral electric field in the channel ($F_{av} = V_{DD}/L_{eff}$) and a different one (F_{max}^{lat} scaling) designed to keep the same value of the maximum lateral electric field at the $Si-SiO_2$ interface. (F_{max}^{lat}) (see Table). In order to estimate intrinsic device performance, a number of parameters have been computed using both the Monte Carlo and the traditional drift-diffusion (DD) model, to compare the results of the two approaches. Fig.6 reports the device transit times (i.e. the channel length divided by the electron average velocity $\bar{v}$), and the cutoff frequency, $f_T = g_m/2\pi C_G$ (where g_m, and C_G are the device transconductance and the gate capacitance respectively), for different length devices, and for F_{max}^{lat} and F_{av} scalings, as calculated using MC and DD

models. Apart from the difference in the absolute values of f_T (18% in the shortest device and higher voltage case) given by the two models, at 0.15 μm the MC simulation predicts an 11% increase in f_T if the F_{max}^{lat} scaling is used instead of the F_{av} one. Under the same conditions the drift-diffusion model gives only a 6% increase in f_T. This pessimistic prediction is essentially due to the effects of velocity saturation which do not really occur at very short gate lengths. Device simulation can also provide the actual average velocity distributions within the device. Results obtained from both MC and DD are shown in Fig. 7, for the case $L_{eff} = 0.15\mu m$. In the case of F_{av} scaling the MC velocity is much higher than DD throughout a large portion of the channel, and this produce a significant enhancement in f_T. However, because the difference in DD and MC velocities is small at the source end of the channel, the MC and DD g_m's are still reasonably close. In the F_{max}^{lat} scaling case, instead, the MC velocities are substantially above those of the DD calculations for the entire channel, and consequently a significant advantage can be taken of velocity overshoot, not only on f_T, but also on current and transconductance. Finally Fig.7 shows that the MC model predicts a much higher increase of $\overline{v}$ than DD if the F_{max}^{lat} scaling is used instead of the F_{av} one: this point is confirmed by the transit time and f_T data of Fig.6.

References

[1] R. Brunetti *et al.*, *Solid State Electron.*, vol. 32, p. 1663, 1989.

[2] A. Abramo *et al.*, in *SISDEP Tech. Dig.*, (Zurich), p. 257, 1991. Hartung-Gorre Verlag.

[3] F. Venturi *et al.*, in *IEDM Tech. Dig.*, p. 503, 1991.

[4] E. Sangiorgi *et al.*, *IEEE Trans. Computer-Aided Design*, vol. CAD-7, p. 259, Feb. 1988.

[5] F. Venturi *et al.*, *IEEE Trans. Computer-Aided Design*, vol. CAD-8, p. 360, Apr. 1989.

[6] C. Jacoboni *et al.*, *Rev. Mod. Phys.*, vol. 55, p. 645, July 1983.

[7] M. V. Fischetti *et al.*, *Phys. Rev. B*, vol. 38, p. 9721, Nov. 1988.

[8] J. Tang *et al.*, *J. Appl. Phys.*, vol. 54, p. 5139, 1983.

[9] T. Vogelsang *et al.*, *J. Appl. Phys.*, vol. 70, p. 1493, 1991.

[10] A. Gnudi *et al.*, in *SISDEP Tech. Dig.*, (Zurich), p. 205, 1991. Hartung-Gorre Verlag.

[11] C. Fiegna *et al.*, in *IEDM Tech. Dig.*, p. 451, 1990.

[12] M. Cohen *et al.*, *Electronic structure and optical properties of semiconductors*. New York: Springer-Verlag, 1989.

[13] G. Gilat *et al.*, *Phys. Rev. Lett.*, vol. 22, p. 715, 1969.

[14] T. Thoma *et al.*, *J. Appl. Phys.*, vol. 69, p. 2307, 1991.

[15] E. Sangiorgi *et al.*, *IEEE Trans. Electron Devices*, vol. ED-39, p. 356, Feb. 1992.

[16] C. Fiegna *et al.*, in *IEDM Tech. Dig.*, p. 119, 1991.

[17] T. H. Ning *et al.*, *J. Appl. Phys.*, vol. 48, p. 286, 1977.

[18] F. Venturi *et al.*, *IEEE Trans. Electron Devices*, vol. ED-38, p. 1895, Aug. 1991.

TABLE

DEVICE PARAMETERS AND BIAS CONFIGURATIONS

L_{eff}	μm	0.75	0.25	0.15	0.075
L_{gate}	μm	1.014	0.316	0.216	0.171
x_j	μm	0.24	0.08	0.08	0.08
N_{Asurf}	cm^{-3}	3.3×10^{16}	1.0×10^{17}	1.0×10^{17}	1.0×10^{17}
N_{Apeak}	cm^{-3}	1.67×10^{17}	5.0×10^{17}	5.0×10^{17}	5.0×10^{17}
t_{ox}	nm	15	5	5	5
Linear Voltage Case $F_{lat} = 80kV/cm$					
V_T	V	0.13	0.25	0.20	0.15
$\left.\begin{matrix}V_{gs}\\V_{ds}\end{matrix}\right\}$	V	6.0	2.0	1.2	0.6
Variable Voltage Case $F_{max}^{lat} = 390kV/cm$					
V_T	V	0.13	0.25	0.20	0.15
$\left.\begin{matrix}V_{gs}\\V_{ds}\end{matrix}\right\}$	V	6.0	2.6	2.3	1.9

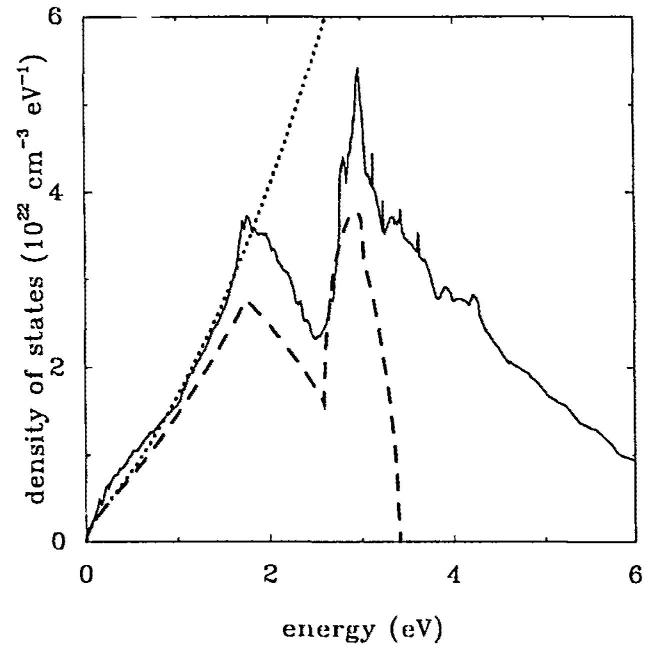

Fig.1: DOS calculated from the model of Ref.[1] (dashed), from the $ASBS$ (solid), and from single non-parabolic band model (dotted).

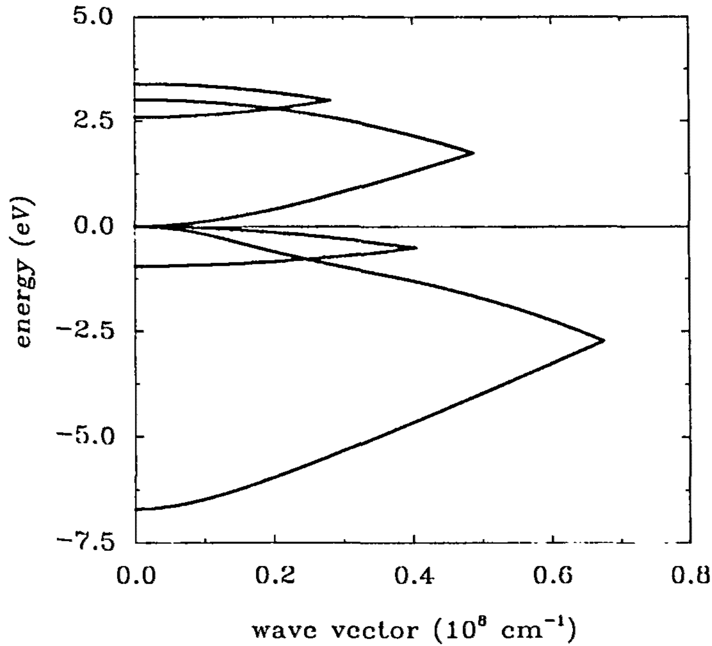

Fig.2: analytical $E(\vec{k})$ for electrons and holes from Refs.[1, 2].

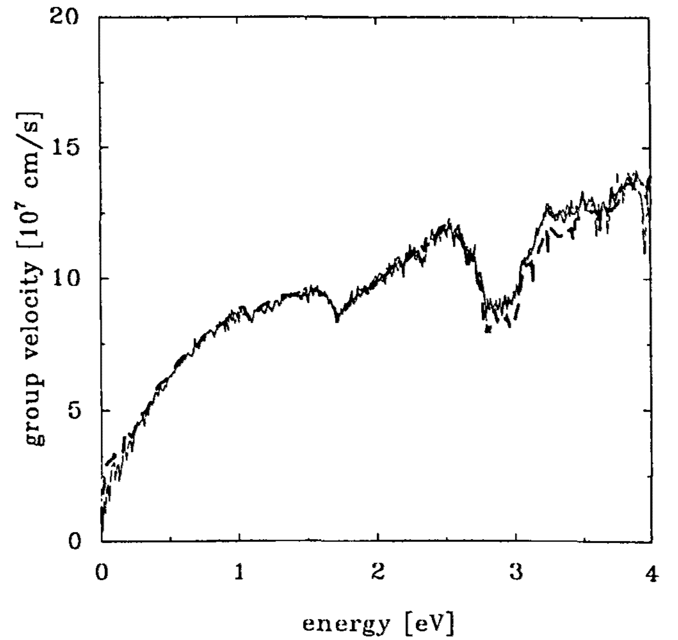

Fig.3: electron $u_g(E)$ from the $ASBS$ (dashed line), and from homogeneous MC simulations using the $ASBS$ [8] (solid lines).

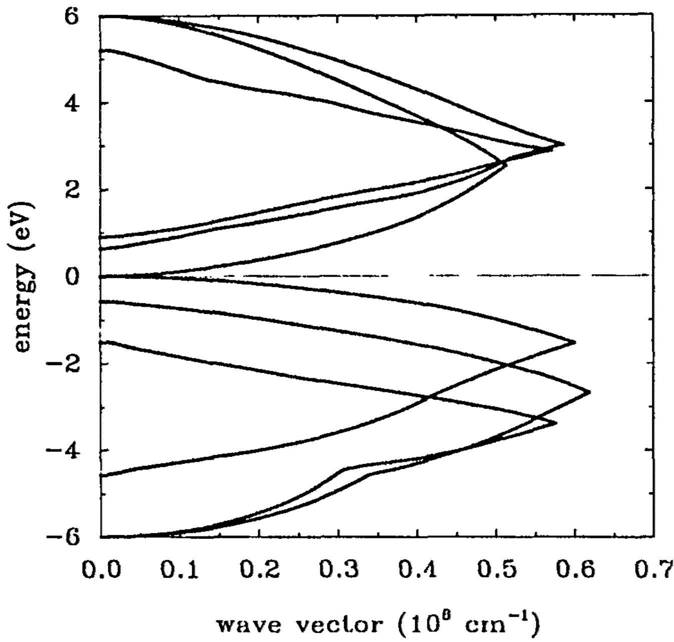

Fig.4: Numerical $E(\vec{k})$ for electrons and holes from Ref.[3].

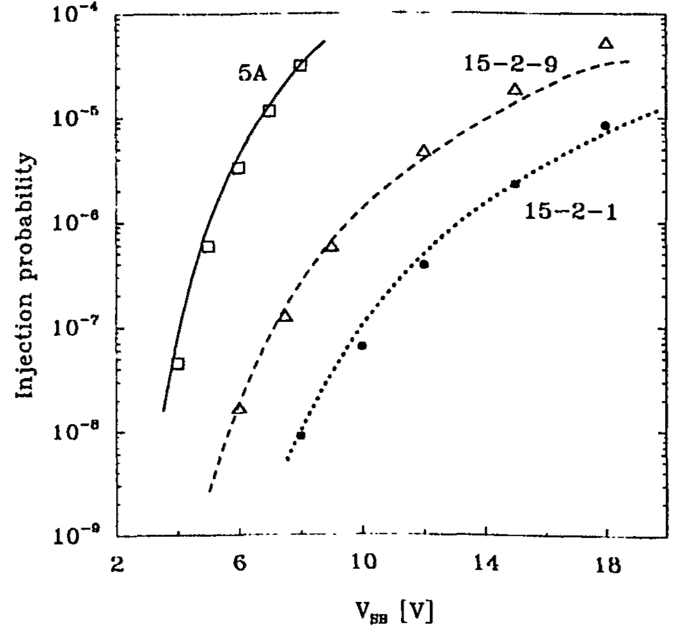

Fig.5: Injection probability vs. V_{SB} and $F_{OX} = 2MV/cm$ for the three different devices labeled 5A, 15-2-9 and 15-2-1 in [17]; lines: experiments; points: simulations.

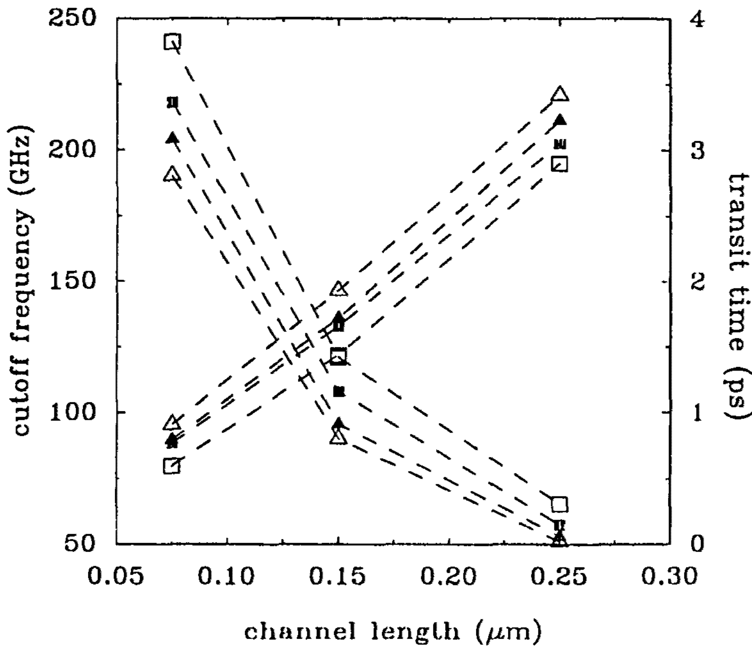

Fig.6: f_T and transit time vs. L_{eff} for two different scalings and the two models. DD, F_{av} scaling (△); DD, F_{max}^{lat} scaling (▲); MC, F_{av} scaling (■); MC, F_{max}^{lat} scaling (□).

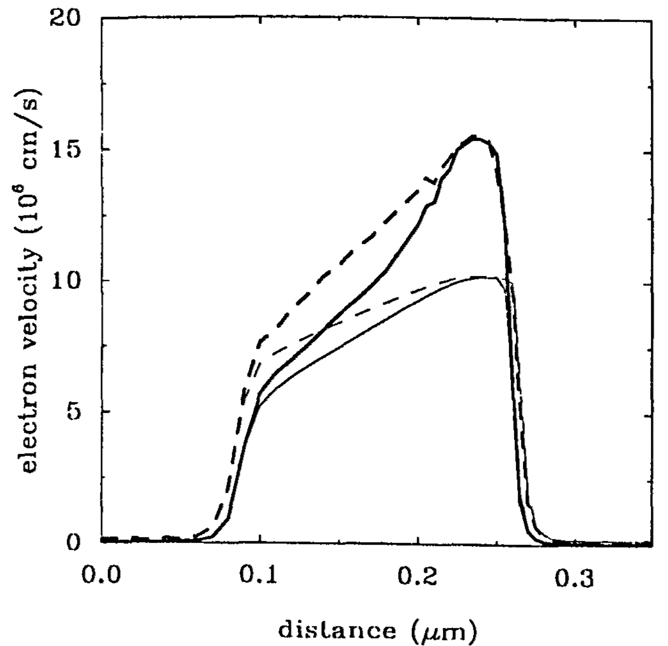

Fig.7: average electron velocity for the device with $L_{eff} = 0.15\mu m$; F_{av} scaling: solid lines; F_{max}^{lat} scaling: dashed lines. MC simulations: thick lines; DD simulations: thin lines.